Biophysical Journal Volume 74 May 1998 2159–2170

A Novel Crystallization Method for Visualizing the Membrane Localization of Potassium Channels

A. N. Lopatin, E. N. Makhina, and C. G. Nichols

Department of Cell Biology and Physiology, Washington University School of Medicine, St. Louis, Missouri 63110 USA

ABSTRACT The high permeability of K^+ channels to monovalent thallium (Tl^+) ions and the low solubility of thallium bromide salt were used to develop a simple yet very sensitive approach to the study of membrane localization of potassium channels. K^+ channels (Kir1.1, Kir2.1, Kir2.3, Kv2.1), were expressed in *Xenopus* oocytes and loaded with Br^- ions by microinjection. Oocytes were then exposed to extracellular thallium. Under conditions favoring influx of Tl^+ ions (negative membrane potential under voltage clamp, or high concentration of extracellular Tl^+), crystals of TlBr, visible under low-power microscopy, formed under the membrane in places of high density of K^+ channels. Crystals were not formed in uninjected oocytes, but were formed in oocytes expressing as little as 5 μS K^+ conductance. The number of observed crystals was much lower than the estimated number of functional channels. Based on the pattern of crystal formation, K^+ channels appear to be expressed mostly around the point of cRNA injection when injected either into the animal or vegetal hemisphere. In addition to this pseudopolarized distribution of K^+ channels due to localized microinjection of cRNA, a naturally polarized (animal/vegetal side) distribution of K^+ channels was also frequently observed when K^+ channel cRNA was injected at the equator. A second novel "agarose-hemiclamp" technique was developed to permit direct measurements of K^+ currents from different hemispheres of oocytes under two-microelectrode voltage clamp. This technique, together with direct patch-clamping of patches of membrane in regions of high crystal density, confirmed that the localization of TlBr crystals corresponded to the localization of functional K^+ channels and suggested a clustered organization of functional channels. With appropriate permeant ion/counterion pairs, this approach may be applicable to the visualization of the membrane distribution of any functional ion channel.

INTRODUCTION

Most if not all techniques developed for labeling and visualization of ion channels are based on labeling of the channel protein itself. These techniques include the use of 1) high-affinity fluorescent or radiolabeled toxins (Froehner et al., 1990; Boudier et al., 1992; Robitaille et al., 1993), 2) immunofluorescent labeling (Shi et al., 1994; Robitaille et al., 1996; Deerinck et al., 1997), and 3) direct fluorescence measurements from channel proteins fused with GFP (green fluorescent protein; Chalfie et al., 1994; Komatsu et al., 1996; John et al., 1997; Veyena-Burke et al., 1997). All of these methods are highly channel specific and are useful for the estimation of channel localization in the presence of other channels. There are, however, several practical disadvantages of these techniques (excluding complexity and price). These include the following: 1) the signal is collected from only a limited number of labeled channels, and in case of low labeling efficiency or bleaching out of GFP, the signal may be lost, and 2) nonfunctional channels and their individual subunits, localized either in the membrane or intracellularly, may contribute to the signal in addition to functional channels. Zampighi et al. (1995) have described a method for estimating the density of membrane proteins in *Xenopus* oocyte membranes based on counting individual complexes on the periplasmic face of freeze-fractured membranes in the electron microscope.

To obtain a specific labeling of functional channels, we have developed a novel approach based on the physical flow of conducting ions through the channel of interest. For one picoamp of ionic current, $\sim 10^6$ ions/s pass through the channel. It is easy to imagine developing a channel labeling method, if only a fraction of these ions could be used to visualize the ion channel. To accomplish this task we have utilized the property of monovalent thallium ($Tl(I)^+$) ions to crystallize at very low concentration with halide ions, such as Br^-. The rationale is that when thallium ions are applied to one side of the membrane, they will pass through the channel pore(s), create a local increase in thallium concentration, and eventually crystallize with Br^- ions that are present on the other side of the membrane. We observe experimentally that crystals grow to visible size, thus marking the location of ion channels on the membrane. Here we present a description of this novel approach, and a second method to confirm hemispheric localization of functional channels, together with early results that demonstrate the application of this method to the study of the polarized distribution of inwardly rectifying potassium channels.

Received for publication 5 November 1997 and in final form 20 January 1998.

Address reprint requests to Dr. A. N. Lopatin, Department of Cell Biology and Physiology, Washington University School of Medicine, 660 South Euclid Ave., St. Louis, MO 63110. Tel.: 314-362-6629; Fax: 314-362-7463; E-mail: anatoli@cellbio.wustl.edu.

0006-3495/98/05/2159/12 $2.00

MATERIALS AND METHODS

Principle of the "crystallization method"

Fig. 1 illustrates schematically the basic principle of the "crystallization method." This very simple assay is based on the unique property of ion

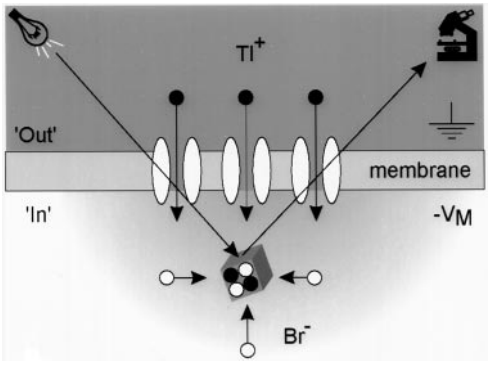

FIGURE 1 K^+ channels can be localized in the membrane by the "crystallization method." When extracellularly applied thallium(I) ions, Tl^+(I), are driven through open K^+ channels into the cell, either by diffusion and/or applied negative membrane potential, they create a local concentration increase that causes crystallization of Tl^+ ions with intracellularly loaded bromide (Br^-) anions. Tl^+ and Br^- ions represent a preferred ion pair compared to K^+ and Cl^-, because Tl^+ is more conductive (Fig. 2) and TlBr is much less soluble than TlCl.

channels being selective pores for certain species of ions—in this case, potassium channels being selective for potassium and certain other related cations. Instead of labeling the ion channel itself with fluorescent toxins, antibodies, or GFP, this method will label the position of the channel. If the channel is exposed to a permeable cation (Tl^+, thallium(I)) at one side of the membrane and to a specific anion (Br^-, bromide, with which Tl^+ forms a poorly soluble salt) at the other side, then the flow of cations through the channel may create a sufficiently high local concentration at the exit of the pore to cause crystallization. Microscopic crystals can then be visualized by microscopy, thus mapping the channel position.

Oocyte expression of K^+ channels

Stage V-VI oocytes were surgically isolated from adult female *Xenopus* under tricaine anesthesia. Oocytes were defolliculated by a 1–1.5-h treatment with 1–2 mg/ml collagenase (Sigma Type 1A; Sigma Chemical, St. Louis, MO) in zero Ca^{2+} ND96 (below). Only oocytes of approximately the same diameter were selected for the purpose of standardization, which is essential for the "agarose-hemiclamp" technique (see below). Two to twenty-four hours after defolliculation, oocytes were pressure-injected with ~50 nl of 1–100 ng/μl in vitro transcribed cRNA encoding for a specific K^+ channel. Oocytes were kept in ND96 + 1.8 mM Ca^{2+} (below) supplemented with penicillin (100 units/ml) and streptomycin (100 μg/ml) for 1–3 days before experimentation.

Loading *Xenopus* oocytes with bromide

Xenopus oocytes expressing K^+ channels (IRK1-Kir2.1, HRK1-Kir2.3, ROMK1-Kir1.1, and DRK1-Kv2.1) were pressure injected (~10% of oocyte volume) with 30 mM potassium bromide (KBr) (to give a final internal concentration of ~3 mM) dissolved in water ~10 min before experimentation, for voltage clamp experiments. Oocytes were then kept in ND96 solution containing 3–30 mM KBr to compensate for the diffusion of Br^- ions out of oocytes.

Electrophysiology

Ionic currents were studied by a standard two-microelectrode voltage-clamp technique with an OC-725 voltage-clamp apparatus (Warner Instruments). Microelectrodes were pulled from thin-walled capillary glass (WPI, New Haven, CT) on a horizontal puller (Sutter Instrument Co., Novato, CA), and tips were mechanically broken to bring electrode resistance to 0.5–2 MΩ when filled with 3 M KCl solution. PClamp software and a Digidata 1200 converter were used to generate voltage pulses and collect data. Data were normally filtered at 5 kHz, digitized at 22 kHz (Neurocorder; Neurodata, New York, NY) and stored on videotape. When necessary, data were redigitized into a microcomputer with Axotape software (Axon Instruments). Leak currents were corrected off-line with a P/1 procedure (+50 mV for Kir2.1 and Kir2.3, −80 mV for Kv2.1) when necessary. Leak currents for Kir1.1 were not corrected. Oocytes expressing Kir channels, with a resting potential of less than −80 mV in low K^+ ND96 solution, were discarded.

When we worked with thallium, care was taken to remove bromide and chloride ions from the bath solution to prevent extracellular precipitation of TlBr or TlCl. KD98 (Cl^- containing) bath solution was completely exchanged for KN98 (NO_3^- containing) solution before applying Tl^+ (NT100). Standard Ag/AgCl grounding electrodes were bathed in 3 M $NaNO_3$ solution and connected to the flow chamber through 1% agar bridges based on the same solution. Glass microelectrodes were filled with 3 M $NaNO_3$.

To grow TlBr crystals of a visible size, oocytes loaded with ~3 mM Br^- (final intracellular concentration) were voltage-clamped in $TlNO_3$ solution (NT100, see Solutions), and 40 to 100 410-ms-long voltage ramps from −80 mV to +50 mV were applied at 0.75-s interpulse intervals. Alternatively, non-voltage-clamped oocytes were loaded with ~30 mM Br^- and then simply incubated with 100 mM Tl^+ (NT100) for ~2 min.

The "agarose-hemiclamp" technique

We have developed the "agarose-hemiclamp" method (Fig. 2) to study the polarized distribution of potassium channels in *Xenopus* oocytes. It is based on direct, and virtually simultaneous, measurement of ionic currents from each hemisphere of an oocyte. Experimentally, one hemisphere is isolated from the other by fixing it in agarose gel prepared with standard KD98 solution while leaving the other side exposed to the flow of the bath solution. In the hemiclamp method, electrodes are impaled in the exposed part of the oocyte. However, in validating the method, we also voltage-clamped completely embedded oocytes (see Results). Completely hardened 1% agar gel does not present any mechanical difficulties for microelectrode movements as long as the electrode is only moved axially during the impalement procedure. The encasement of the membrane in agarose gel does not affect ionic currents through the membrane (see Results), but dramatically slows down access of bath solution to the isolated area, access requiring ion diffusion through the agar. The conductance in 2 mM extracellular K^+ is considerably decreased compared to conductance in 100 mM K^+ (KD98), and current amplitude is almost zero with 2 mM extracellular K^+ at ~ −80 mV membrane potential, because it is very close to the K^+ current reversal potential. Therefore, when high K^+ bath solution (KD98) is rapidly substituted for low K^+ (ND96) bath solution, the amplitude of ionic current at −80 mV (close to E_K) changes from that of the whole oocyte to that originating from the part of the oocyte that is immersed in the agarose gel (and hence still exposed to ~100 mM K^+), thus allowing estimation of the ion channel distribution.

To encase only one hemisphere in agarose, *Xenopus* oocytes were appropriately positioned in ~0.5-mm-deep holes and then covered with freshly prepared 0.5–1% agarose (Type II-A; Sigma) in KD98 at ~35–37 C°. After 2–10 min of hardening at 4°C, the gel-embedded oocytes were carefully detached from the base, and individual oocytes were cut out and voltage-clamped, as shown in Fig. 2.

Image handling

Images of oocytes were obtained with an Olympus OM-2 camera attached to a dissecting microscope (Nikon SMZ-1B; Nikon, Japan). Photo prints were digitized and imported to a CorelDraw 5.0–6.0 graphics package for presentation. Confocal images of oocytes were obtained with a Biorad MR 1000 confocal microscope by illumination with 548-nm yellow light from

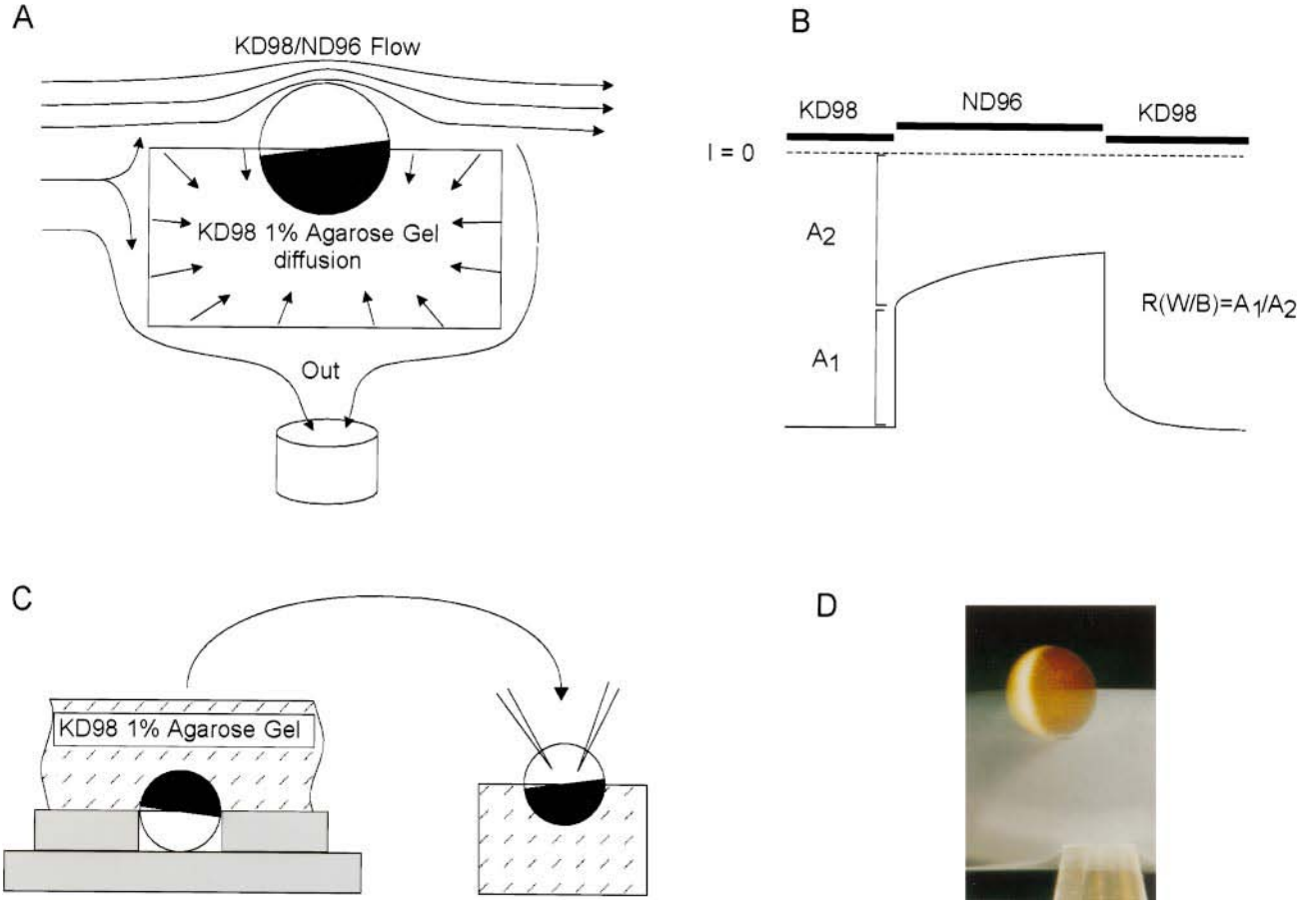

FIGURE 2 Ionic currents from different hemispheres of *Xenopus* oocytes can be separated by the "agarose-hemiclamp" technique. (*A*) If one-half of an oocyte is embedded in 1% agarose gel based on high K^+(KD98) solution, then bath solution can only reach the embedded half of the membrane by diffusion, while the free half of the membrane can be accessed by fast application of the desired solution. (*B*) When the bath solution is rapidly changed from high [K^+] KD98 to low [K^+] ND96, the current amplitude will drop from its full magnitude ($A_1 + A_2$) to that originating only from the embedded part of the oocyte (A_2). Distribution of functional ion channels can then be estimated as the ratio $R = A_1/A_2$. (*C*) Procedure for embedding oocytes into agarose gel (see Materials and Methods). (*D*) An arbitrarily positioned *Xenopus* oocyte ~50% embedded into 1% KD98-based agarose gel. The tube visible at the bottom of the picture is used as a suction holder for manipulating the gel piece.

an argon laser and capturing reflection from TlBr crystals. Image Tool (UTHSCSA, V-1.27) and CorelDraw PhotoPaint software were used for image analysis.

Solutions

The solutions used in these experiments had the following compositions:

NT100: 100 mM $TlNO_3$, 1 mM $Mg(OH)_2$, 5 mM Na · HEPES, pH ~7.4 with NaOH

KN 98: 98 mM KNO_3, 1 mM $Mg(OH)_2$, 5 mM K · HEPES, pH ~7.4 with KOH

ND 96: 96 mM NaCl, 2 mM KCl, 1 mM $MgCl_2$, 5 mM Na · HEPES, pH ~7.5 with NaOH

KD 98: 98 mM KCl, 1 mm $MgCl_2$, 5 mM K · HEPES, pH ~7.5 with KOH.

RESULTS

Ionic currents in thallium-containing solutions

Several potassium channels are more permeable to monovalent thallium (Tl^+) ions than to K^+ (Hagiwara et al., 1977; Blatz and Magleby, 1984; Eisenman et al., 1986; Wagoner and Oxford, 1987; Oxford and Wagoner, 1989; Chepilko et al., 1995; Cloues and Marrion, 1996), although for many potassium channels the actual Tl^+ conductance is less than K^+ conductance (Eisenman et al., 1986; Chepilko et al., 1995; Cloues and Marrion, 1996). Not only are native strong inward rectifier channels more permeable to Tl^+ ions; they also conduct more current when Tl^+ is completely substituted for K^+. Fig. 3 shows that in *Xenopus* oocytes expressing Kir2.3 channels, inward current is more than doubled in amplitude and reversal potential shifts to more positive values when extracellular thallium is substituted for potassium. The shift of reversal potential is $+16.4 \pm 2.2$ mV ($n = 5$) for Kir2.3 and $+10.0 \pm 0.4$ mV ($n = 5$) for Kir1.1 channels, giving a relative permeability ratio P_{Tl+}/P_{K+} of 1.9 and 1.5, respectively, using the Goldman-Hodgkin-Katz equation (Hille, 1992). Data on membrane conductance in Tl^+ containing solutions may represent lower estimates because, in the presence of Tl^+, current

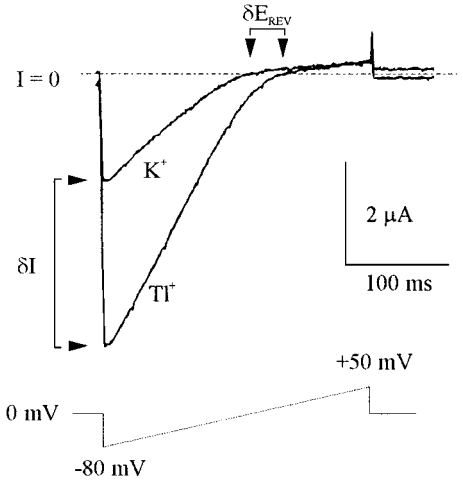

FIGURE 3 Monovalent thallium, $Tl(I)^+$, is a more permeable and a better conducting ion than K^+. HRK1 (Kir2.3) channels were expressed in *Xenopus* oocytes, and ionic currents were recorded using a two-microelectrode voltage clamp in response to ~400-ms voltage ramps from −80 mV to +50 mV in the presence of 100 mM extracellular (*1*) KNO_3 or (*2*) $TlNO_3$ (~1 min after switching from K^+-containing solution). Both an increase of inward current (δI) and a positive shift of reversal potential (δE_{REV}) are observed in Tl^+ solution (typical result from $n = 5$ oocytes).

amplitudes usually decline with time, without change in reversal potential. There was no measurable recovery upon complete washout of extracellular Tl^+, at least within a few minutes. Although we have no explanation of this phenomenon, at high current densities (more than 20 μA at −80 mV per oocyte), and frequent pulsing, fine white crystals of TlCl can actually be observed under a dissecting microscope (not shown), and these TlCl crystals also did not disappear after washout of Tl^+.

To minimize Tl^+ entry, the membrane potential was continuously held at 0 mV (close to the reversal potential) when the bath solution was changed from K^+- to Tl^+-containing solution.

An extrasensitive assay for membrane localization of functional potassium channels

Simple calculations assuming free diffusion of permeating ions in bulk solution predict that a 1-pA ion current flowing through a 10-Å-wide channel could generate a local ion concentration of several millimolar inside the channel mouth (see Appendix). Given the low solubility of TlBr, a millimolar local concentration of Tl^+ ions would be sufficient to form TlBr crystals with Tl^+ ions entering through a single ion channel, with millimolar intracellular Br^-. Thus, under appropriate conditions, localization of K^+ channels can be visualized by observation of TlBr crystals. One example of such an experiment is shown in Fig. 4. *Xenopus* oocytes were injected with ~5 ng of Kir2.3 cRNA into the animal (dark) hemisphere (pole), which resulted in whole-oocyte currents in the range of 1–20 μA (after 1–3 days of incubation) at −120 mV membrane potential. Oocytes were then injected with ~50 nl of 30 mM KBr to bring intracellular concentration to ~3 mM and voltage-clamped with a two-microelectrode voltage clamp in thallium-containing solution (NT100; see Materials and Methods). Forty × 410 ms linear voltage ramps from −80 mV to +50 mV were applied at a frequency of 0.75 Hz to drive the inward flow of Tl^+ ions, ionic currents were recorded, and oocytes were photographed periodically. In the particular oocyte shown in Fig. 4, *A–C*, multiple white crystals formed in a large patch on the dark (animal) hemisphere and were easily observed under the normal light conditions used in dissecting microscopes. In another example (Fig. 4 *E*), crystals are more clearly grouped into a patch located on the animal (dark) part of the oocyte. These "white spots" were not observed in oocytes injected with water, or in oocytes with very low (less then ~0.2 μA at −80 mV) expression of K^+ channels (under the same protocol) or in K^+ channel expressing oocytes clamped to voltages at which channel open probability is low (i.e., ~20–50 mV positive to E_K for Kir2.1 and Kir2.3). A small number of relatively large crystals scattered around the whole oocyte could be observed in "damaged" nonexpressing oocytes, if they displayed large (i.e., a few μA at ± 50 mV) leakage currents. Crystal growth could also be observed around the current or voltage electrodes if the membrane was damaged during impalement (Fig. 4 *D*), or when "nondamaged" oocytes were subjected to oscillations resulting from induced instability of the voltage-clamp feedback loop, which is known to cause electrical damage of the oocyte membrane and subsequent development of current leakage through nonselective membrane holes. Much finer crystals could also be observed in K^+ current-expressing oocytes without intracellular bromide, at high current densities (>20 μA at −80 mV), due presumably to the formation of TlCl crystals (not shown).

TlBr crystals are also formed in similar experiments with Tl^+ flowing through strong inward rectifier IRK1 (Kir2.1), weak inward rectifier ROMK1 (Kir1.1), and delayed outward rectifier DRK1 (Kv2.1) channels (results not shown). Patches of white crystals are easily observed in nonclamped oocytes expressing K^+ channels, if the oocytes are preinjected with a higher concentration of bromide (300 mM, to achieve a final intracellular concentration of ~30 mM) and then simply incubated with thallium. Taken together, the results indicate that in nondamaged oocytes expressing K^+ channels, crystals form under the membrane because of the interaction of intracellular Br^- with Tl^+ ions flowing through the channels.

TlBr crystals are preferentially located at the point of cRNA injection

It was clear after initial experiments that patches of TlBr crystals are not arbitrarily scattered on the surface of oocytes but are typically located around the point of cRNA injection, as shown in Fig. 5. When cRNA was injected in

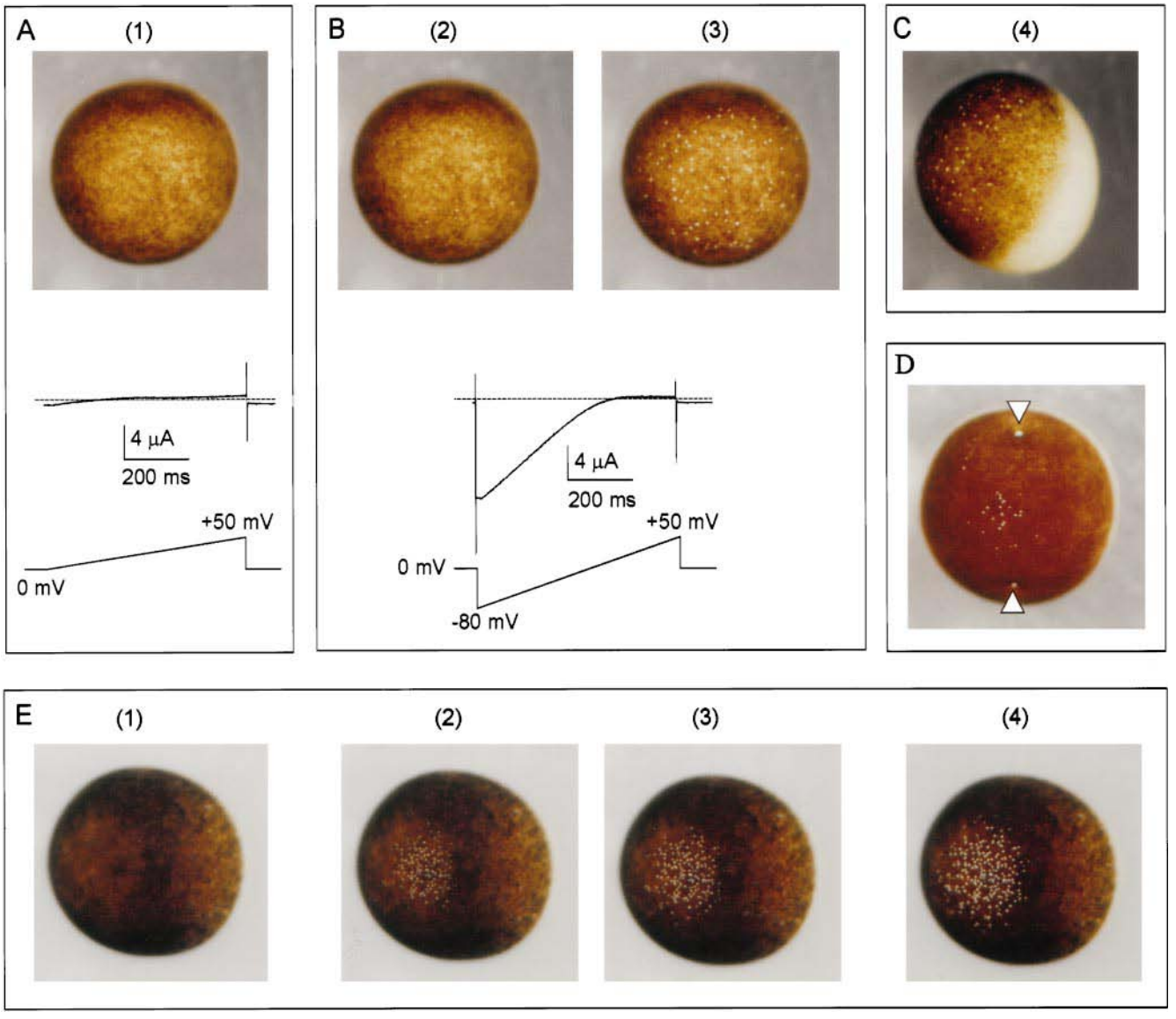

FIGURE 4 Crystal growth is determined by flow of Tl^+ ions through K^+ channels. *Xenopus* oocytes (injected with cRNA into the animal pole) expressing HRK1 (Kir2.3) channels were loaded with bromide ions by microinjection (~0.3 mM final intracellular concentration) and voltage-clamped at 0 mV. Extracellular $TlNO_3$ (100 mM) was substituted for KNO_3 and voltage ramps (as indicated) applied at 1.5 Hz frequency. (*A*) (*1*) Oocyte image taken after ~50 voltage ramps, from 0 to 50 mV (no net inward current). (*B*) To increase inward flow of Tl^+ ions, voltage ramps from −80 to +50 mV were then applied and pictures were taken after the 20th (*2*) and 40th (*3*) ramps. Zero current is indicated by the dashed line. (*C*) The same cell was unclamped and tilted. (*D*) In a similar experiment, white TlBr crystals were formed with time around the point of microelectrode impalement (*arrowheads*). (*E*) In an experiment similar to that in *A*, a smaller patch of crystals is observed.

the animal (dark) pole, crystals formed in that hemisphere. Conversely, when cRNA was injected into the vegetal (light) hemisphere, crystals were formed in that hemisphere. We call this specific arrangement of TlBr crystals due to localized injection of cRNA a pseudopolarization, as opposed to natural polarization discussed later in the paper. This phenomenon seems to be rather persistent because pseudopolarization did not disappear within 1–3 days after injection of cRNA. Furthermore, incubation of oocytes with a mixture of 1 μM cytochalasin B and 1 mM colchicine for 1–3 days failed to destroy pseudopolarization ($n = 5$ oocytes), although the color pattern of oocytes deteriorated almost completely within this period (not shown).

Direct evidence for colocalization of functional K^+ channels and TlBr crystals

One reasonable criticism of the crystallization technique described above would be that localization of TlBr crystals is merely a reflection of disturbances in the membrane of the oocyte caused by the damaging procedure of cRNA injection, rather than a reflection of the real distribution of functional ion channels. Several possible approaches might be used to prove that the distribution of TlBr crystals reflects the distribution of functional K^+ channels. It could be done, for example, by labeling the channel protein by conventional techniques involving fluorescent antibodies,

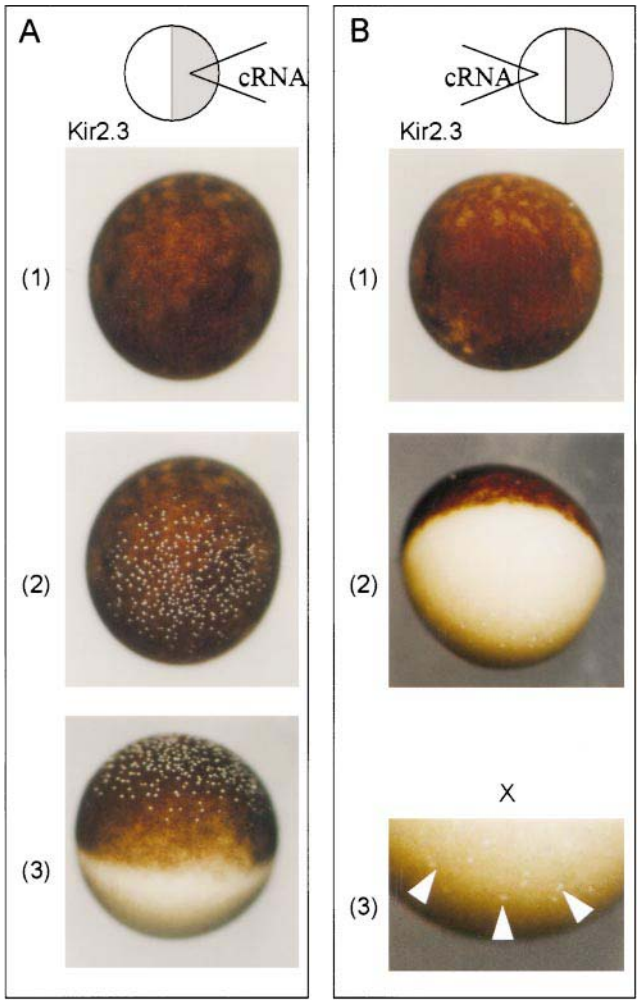

FIGURE 5 Pseudopolarization of K^+ channel distribution is due to localized injection of cRNA. *Xenopus* oocytes were injected with HRK1 (Kir2.3) cRNA at the animal (*A*) or at the vegetal (*B*) pole and allowed ~36 h for channel expression. Oocytes were then loaded with a ~3 mM final intracellular concentration of Br^- ions and voltage-clamped in thallium-containing (NT100) solution. Images were taken (*1*) after ~40 voltage ramps from 0 mV to +50 mV and (*2*) after ~50 voltage ramps from −80 to +50 mV. Oocytes were then unclamped and tilted (*3*). Arrowheads point to TlBr crystals located on the vegetal side of the oocyte.

toxins, or GFP-tagged fusion ion channels. Although very specific to the channel protein subunit itself, these approaches all suffer from the same principal problem—they are not specific for functional channels. It is clear, at least in some cases, that the distribution of a protein may not correspond to the distribution of its function (Matus-Leibovitch et al., 1994). Hence the only direct way to study distribution of functional protein complexes is to study the distribution of their function itself. For ion channels this means direct assessment of ionic currents at different membrane locations.

To directly measure K^+ currents in separate hemispheres of *Xenopus* oocytes, we have developed the agarose-hemiclamp technique (see Materials and Methods), based on the capacity of agarose to electrically conduct ions as well as free solution while obviating the bulk flow of ions, ensuring that the embedded part of the oocyte is isolated from fast changes of the bath solution (Fig. 2). In Fig. 6 *A*, an oocyte expressing Kir2.3 channels was first voltage-clamped in KD98 solution, and two microelectrodes were used to record K^+ currents. The clamp circuit was then switched off, the electrodes were removed, and the oocyte was completely embedded in 1% agar in KD98. After the agar had set and cooled to room temperature, the piece of gel containing the oocyte was cut out and the oocyte was voltage-clamped again. The currents in agar (*b*) were virtually indistinguishable from the control currents (*a*), except for a slight increase in leakage current. Similar results were obtained in three other oocytes. This experiment confirms one of the major premises of the technique: that channels remain functional and their properties are essentially unchanged during the embedding procedure. Fig. 6, *B* and *C*, shows currents recorded from two oocytes that had been injected with Kir2.3 cRNA in the light (vegetal) pole, and either the light (vegetal, *left*) or dark (animal, *right*) hemispheres were embedded in KD98-agarose. In both cases large (10–20 μA) inward currents (at −80 mV) are evident when the oocytes are first voltage-clamped with KD98 solution in the bath. With the vegetal hemisphere (i.e., the injected hemisphere) embedded, large currents persisted after the bathing solution was switched to low K^+ ND98 solution (*C*, *left*), but with the animal hemisphere embedded, K^+ currents almost disappeared when the bath solution was switched to ND96 (containing 2 mM K^+; *C*, *right*). This indicates that the active channels were present almost exclusively in the light (vegetal) hemisphere. Pseudopolarization is so strong that virtually no currents can be measured on the side of the oocyte opposite to that in which the cRNA was injected. Opposite channel distributions were obtained with injection in the dark (animal) pole, and recording was done with either animal or vegetal hemispheres immersed in agarose. The average pseudopolarization, estimated as the ratio between the current recorded from the pole of injection (current in ND96/current in KD98, injected hemisphere exposed to bath) and the current recorded from the whole oocyte (current in KD98) was $R = 0.97 \pm 0.02$ ($n = 2$ and 4, for animal and vegetal injections, respectively). One immediate practical conclusion from these results is that to obtain maximum patch-clamp current density, cRNA should be injected into one specific pole and membrane patches should be isolated from the same hemisphere.

Although technically difficult, several successful experiments using the giant pipette patch-clamp technique were carried out to directly measure ionic currents from patches including a single visible macrocrystal under the patched membrane. The results provide further evidence for a polarized and clustered organization of K^+ channels. From oocytes expressing only a few microamps of current (at −80 mV, KD98 extracellularly), amplitudes from 10 to 20 nA ($n = 3$) were measured from patches with captured visible (~30–50 μm) crystals, those from 0.1 to 0.5 nA ($n = 3$) were from patches formed between visible crystals

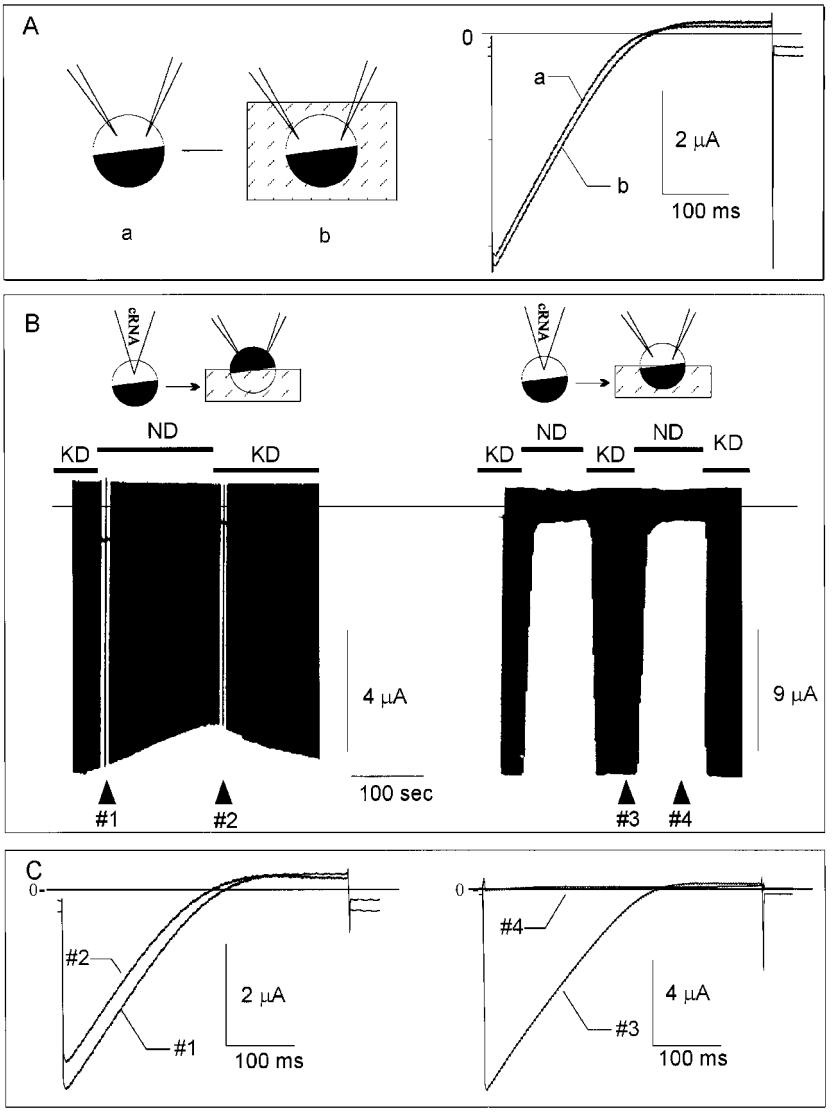

FIGURE 6 Strong pseudopolarization can be directly measured by the "agarose-hemiclamp" technique. (*A*) Ionic currents through HRK1 (Kir2.3) channels are essentially unaffected when the oocyte is embedded in agarose gel, as is evident from current measurements taken before (*a*) and after (*b*) the embedding procedure. (*B*) *Xenopus* oocytes were injected with Kir2.3 cRNA at the vegetal pole ~36 h before experimentation, and then ~50% embedded into 1% KD98 agarose gel with the vegetal (*white*) side exposed to the bath solution or gel as indicated. Oocytes were voltage clamped, and the bath solution was changed as indicated from high K^+ (KD) to low K^+ (ND), and back and ionic currents in response to 410-ms-long voltage ramps from −80 mV to +50 mV were recorded (*C*).

(therefore potentially containing only multiple invisible ones), and virtually zero current (less than 50 pA) was from the hemisphere opposite that which was injected ($n = 5$).

Crystals can be visualized by confocal microscopy to enhance image contrast and to observe out-of-focus regions

The usefulness of photographed oocyte images obtained by ordinary light microscopy is limited by 1) low image contrast (especially for crystals located on the white, vegetal side), and 2) low depth of focus, which prevents more detailed analysis of crystal localization. However, because of the macro size of TlBr crystals and their relatively high reflective properties, reflection confocal microscopy can be successfully applied for oocyte imaging (Fig. 7 *A*). Fig. 7 *B* shows a representative series of selected confocal "slices" taken from the vegetal (white) hemisphere of oocytes expressing Kir2.1 channels, and their total ("piled-up") projection is shown in Fig. 7 *C*. Although Fig. 7 *C* illustrates the most typical, uniform pattern of functional channel distribution that is observed, some oocytes display a very peculiar crystal arrangement in the absence of any visual disturbances in the color pattern of the oocyte. For example, Fig. 7 *D* shows the total projection of confocal images from another oocyte with clearly observed "spots of silence" (*arrowheads*) in places distant from the points of injection of cRNA and bromide and, thus, not easily explained as an artifact of the crystallization method. In some images taken at higher magnification, it was also possible to observe apparently circular paths along which TlBr crystals were located (not shown).

There is a visual illusion that the crystal pattern consists mainly of large (>1-μm diameter) crystals of virtually the same size. Quantitative analysis of a small (~200 × 200 μm) area (to avoid errors due to polarized channel distribution) shows, however, that the distribution of their sizes is well approximated by an exponential function (Fig. 7 *E*).

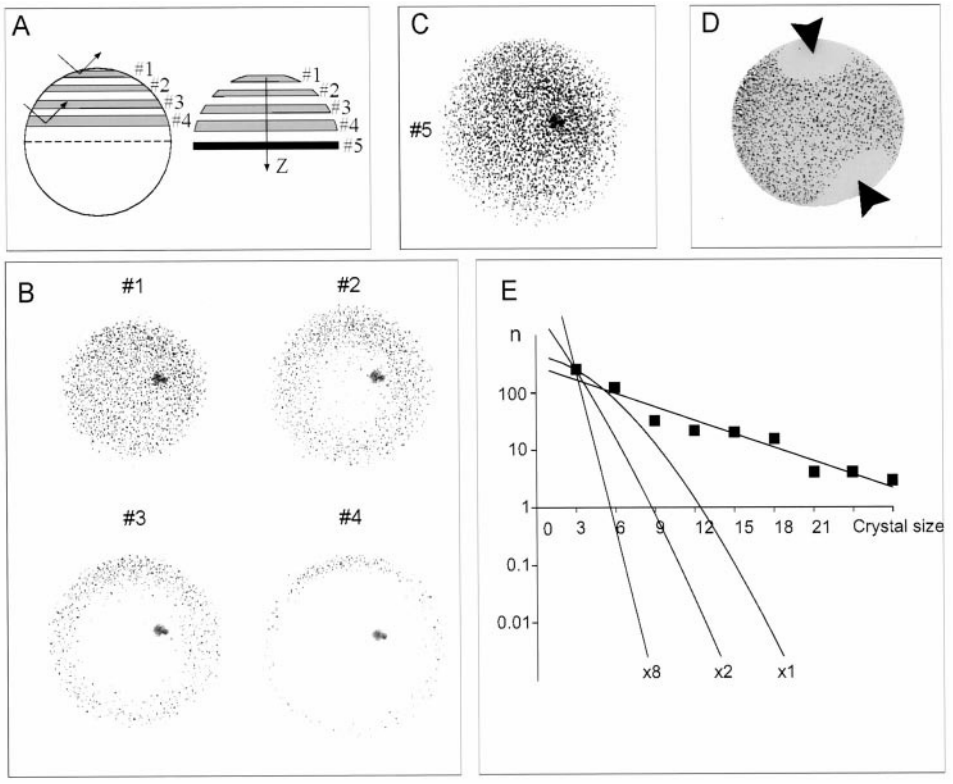

FIGURE 7 Reflection confocal imaging of TlBr crystals in *Xenopus* oocytes. (*A*) Reflected light from TlBr crystals can be collected at different (*z*) depths (*1, 2, 3,* and *4*) by confocal microscope and finally projected into a single "piled-up" image. (*B*) Selected confocal images were taken at $z \approx 20$ (*1*), 80 (*2*), 200 (*3*), 300 (*4*) μm from the top of an oocyte expressing ROMK1 (Kir1.1) channels and treated as described in Materials and Methods to grow TlBr crystals. The *Z* resolution (3.4× objective and iris diaphragm $I = 8$) was set to minimum for the purpose of presentation. (*C*) The "piled-up" image (*5*) obtained for the same oocyte. (*D*) In the absence of any visual disturbances in the color pattern of oocytes, unusual distributions of active channels can be observed. This "piled-up" image was obtained from a non-voltage-clamped oocyte that had been injected in the visualized hemisphere. Two areas without crystals (*arrowheads*) are observed. (*E*) Observed distributions (*n*) of crystal size (area in pixels), fitted with an exponential function, and theoretical predictions assuming a random distribution (Poisson equation) of channels. The experimentally observed distributions are a much shallower function of crystal area than predicted for a random distribution. *×1, ×2, ×8* indicate theoretical minimal sizes (1, 2, or 8) of channel clusters needed to initiate crystallization (see Discussion).

The exponential decline is rather shallow, i.e., the number of crystals of a bigger size (area on the graph) is reduced approximately twofold with doubling of their size. Superimposed on this graph are predicted distributions of crystal size calculated with the Poisson equation, which assumes a random (not clustered) distribution of ion channels in the membrane. Clearly, the slope of theoretical predictions is much steeper than that found experimentally, arguing against a random channel distribution (see Discussion).

Naturally polarized distribution of functional ion channels

Xenopus oocytes (stages V and VI in this study) are polarized cells. In addition to the obvious color pattern, there exists a deeper asymmetry, including closer localization of germinal vesicle (nucleus) to the animal part of the oocyte, and asymmetrical distribution of structural (Palecek et al., 1985) and functional proteins (Kume et al., 1993). To study how the natural polarization of the oocyte might affect the distribution of exogenously expressed K^+ channels, the phenomenon of pseudopolarization described above has to be taken into account. Therefore, we injected K^+ channel cRNAs at the oocyte equator (i.e., the junction of the animal and vegetal poles), and assayed the subsequent distribution of K^+ channels by confocal imaging of TlBr crystals. At the time of cRNA injection, care was take to position the injection electrode at the equator and perpendicular to the surface of each oocyte. In virtually every experiment carried out at the beginning of this study, we found a pronounced, natural polarization of K^+ channels, in the vegetal (white) hemisphere. In later experiments, natural polarization was less obvious (more than 100 oocytes were studied in total), and some oocytes exhibited no obvious polarization. We never observed reversed natural polarization with channels located primarily in the animal (dark) hemisphere. We cannot offer any immediate convincing explanation for the lack of reproducibility in later experiments. However, we did observe that natural polarization existed either in most of the oocytes from a given isolation, or in none of them, suggesting that such polarization depended on the condition of the donor frog, or on some uncontrolled variable in the

isolation procedure. Quantitative analysis of oocyte images also confirms that most of the crystals are observed on the vegetal side. Digital confocal images were analyzed pixel by pixel, and polarization was estimated as the ratio R_{pol} between the fraction of pixels containing TlBr crystals on the vegetal side and the fraction of TlBr containing pixels on the animal side. Polarization was $R_{pol} = 9.15 \pm 3.4$ for Kir2.1, $n = 25$; $R_{pol} = 13.6 \pm 8.4$ for Kir2.3, $n = 16$; $R_{pol} = 22.9 \pm 6.2$ for Kv2.1, $n = 9$.

DISCUSSION

Potential applications of the crystallization method and the agarose-hemiclamp technique: demonstration of channel polarization

Although the idea of forming crystals at the location of a channel, by allowing permeating ions to precipitate an insoluble salt on meeting an appropriate counterion on exiting the channel, is a simple one, we are unaware of this approach being utilized before. The results presented above demonstrate that it is a feasible approach to examining the distribution of potassium channels on the surface of *Xenopus* oocytes, and provides useful information regarding the polarized distribution of inward rectifier and delayed rectifier K channels exogenously expressed in this system. A generally neglected point, when other localization methods, such as antibody labeling, are used is the potential complication that such methods label proteins and not functional units. GFP-tagged proteins, for instance, are detected whether they are at the surface or are intracellular (Makhina and Nichols, 1998). Chemical ligands can label nonfunctional proteins, as well as functional complexes at the cell membrane (Matus-Leibovitch et al., 1994). For labeling functional channels, the present method should therefore, in principle, be preferable to other such indirect methods.

In principle, this approach of using thallium halide crystal formation could specifically be extended to the examination of potassium channel distributions in any cell type. Moreover, by appropriate choice of other permeant ions, and counterions to generate insoluble precipitates, the approach should be applicable to examination of the distribution of any other ion-selective channel. We have begun preliminary experiments to examine crystal formation in cell lines expressing cloned K channels. In such cells, crystals are formed, although high background crystal generation (i.e., in untransfected cells), which may result from high levels of endogenous pathways for either the permeant ion or the counterion, have thus far not permitted us to observe channel-specific crystal formation.

The agarose-hemiclamp method is a simple application of the principle that agarose conducts ions as well as free solution, but the immobility of the medium means that bulk ion flow does not occur, and diffusion is very slow. The large size of oocytes makes them very suitable for the approach, relying only on having an appropriately sized hole in a plexiglass chamber to allow the oocyte to make a physical seal that is tight enough to exclude the flow of molten agar. The results presented above demonstrate the simple feasibility of the approach, and very nicely confirm the pseudopolarized distribution that we see with TlBr crystal formation. In combination with our demonstration that ion channels (and probably by extrapolation, other membrane proteins) reproducibly show profound pseudopolarization, this approach might be very useful for investigation of the indirect interactions between, say, a receptor expressed in one hemisphere and an effector channel or other protein expressed in the opposite hemisphere.

Potential limitations of the crystallization method: theoretical considerations

The principal difficulty in employing this novel approach is in the nature of crystal growth. Crystal growth in any medium is initiated from microscopic nuclei ("seeds") that randomly appear in either supersaturated or supercooled solutions. Qualitatively, any new phase (crystal nucleus) would have an enhanced solubility when first formed, because of its tiny size, and would immediately disappear rather than grow to a larger size. The radius of a minimal stable seed can be estimated:

$$r = \frac{2\sigma \cdot M}{dRT \ln \alpha}$$

where α expresses the supersaturation as a concentration ratio, d is the density, σ is the interfacial tension, M is the molar volume, and r is the radius of an isotropic spherical nucleus in equilibrium with supersaturated solution. Numerical estimations for the sizes of critical nuclei, for vapors, melts, or water solutions, all fall within the 10–20-Å range (Van Hook, 1961), or are even less for slightly soluble salts (assuming steady-state supersaturation values, which are usually in the range of 2–10). Therefore, the relevant nucleus size might be small enough to be within the scale of individual protein dimensions. This estimation is below the resolution of light microscopy and suggests that individual channels might, in fact, be resolvable by electron microscopy. A problem, however, is that when a newly formed crystal begins to grow, it will effectively reduce the concentration of precipitating ions (Tl^+ and Br^-) around itself, thus reducing the probability that another nucleus will appear. Therefore, depending on the specific conditions of the experiment, there should exist a minimum characteristic distance (we will call it the "spatial resolution") between nuclei. The situation is very reminiscent of that in photography, where film space resolution (granularity) is defined by the distance between $AgNO_3$ microcrystals and their size. Prediction of the spatial resolution in the present context is virtually impossible, because of the undefined conditions of crystallization inside a living cell. However, general expectations based on experimental observations are possible, taking into account the timing properties of nucleation and supersaturation. For the critical size of the nu-

cleus, one can estimate the work of nucleation, W, and hence the rate of nucleus formation (Van Hook, 1961),

$$v = k\exp(-W) = k\exp\left[-\frac{16\pi\cdot M^2\sigma^3}{3d^2R^3T^3\ln^2\alpha}\right]$$

with parameters as discussed above. This expression illustrates the "explosive" increase in the rate of nucleation as the solution achieves a critical degree of saturation (i.e., as α exceeds a certain value). Increasing the temperature (cubic function), and thus indirectly reducing the interfacial tension of the crystal (cubic function), is also favorable. As demonstrated experimentally, supersaturation is easy to create, even with intracellular bromide anions at a concentration as low as ~3 mM, and this concentration could be increased at least 10-fold without significantly affecting ionic balance in the oocytes. The frequency factor (k) is not easily calculated, although the experimental observation that crystallization in oocytes can happen within seconds (and probably much faster) obviates conclusion. Faster and greater supersaturation and hence higher spatial resolution could be achieved by using other anions that generate salts of lower solubility with thallium. Thallium iodide (TlI), for example, is much less soluble than TlBr (Table 1; X^- is the concentration of the precipitating anion at 1 mM thallium), and selenides are virtually insoluble. Free selenium and sulfur ions, however, are not stable and tend to be very reactive chemically, and therefore we have not used them in this first study. In initial experiments with voltage-clamped oocytes, we did observe membrane crystals formed from permeating thallium meeting internally injected iodide. However, we also routinely observed progressively increasing leakage currents, and crystal formation around the voltage-clamp electrodes, perhaps due to some specific effect of TlI crystals on the membrane. In nonclamped oocytes (i.e., without embedded electrodes), "powdery" crystals were observed on the oocyte surface, but the size of these microcrystals was too small to reliably resolve them on the highly reflective granular background of the oocyte surface using reflection microscopy. Preliminary experiments with cultured BHK cells suggest, however, that the size and distance between TlI crystals (the spatial resolution) that form because of the flow of Tl^+ and/or I^- through endogenous ion channels may be in the submicron range (not shown). Several other complex counterions, such as $Cr_2O_7^-$ or MoO_4^-, also produce barely soluble salts with Tl^+ ions and are currently under investigation.

TABLE 1 Relative solubilities of selected thallium and selenium compounds

Compound	Sol. g/100 cm^3	[C] mM	X^- at 1 mM [Tl^+]
TlBr	0.05	1.76	3.1
TlI	0.0006	0.018	0.00032
Tl_2S	0.02	0.45	0.36
Tl_2Se	Insoluble		

Are K^+ channels clustered on *Xenopus* oocyte membranes?

Clustering of ion channels implies a specific interaction at the molecular level. Such molecular-level clustering can only be resolved if channel aggregates are bigger than the resolution of the microscopy that is employed. There are several reports of such aggregation of ion channels, one of the best studied examples being the clustering of ACh receptors by the 43K/rapsyn synapse-associated intracellular protein (Froehner et al., 1990; Phillips et al., 1991). Kim et al. (1995) showed that macroscopic (~0.5–2 μm) patches of voltage-gated Kv1.4 potassium channels can easily be observed in COS7 cells when the channel is coexpressed with PSD-95 protein. In these experiments, PSD-95 failed to cluster Kv4.2 channels; however, clustering of these channels in native neuronal membranes has been demonstrated by immunostaining techniques (Alonso and Widmer, 1997). Delayed rectifier Kv2.1 K^+ channels are arranged in large clusters in mammalian central neurons or when exogenously expressed in polarized MDCK cells but not in COS-1 cells (Scannevin, 1996), as judged by immunofluorescence. It should be straightforward to confirm by direct patch-clamp current measurements that such macroscopic clustering of channel proteins correlates with channel function, although such studies have not been performed. Shi et al. (1994) have shown, using immunogold electron microscopy, that delayed rectifier (Kv2.1) K^+ channels expressed in COS-1 cells are probably clustered on a microscopic level. In contrast, no clustering of *Shaker* K^+ channels (using a nonconducting mutant) expressed in *Xenopus* oocytes was detected by freeze-fracture electron microscopy (Zampighi et al., 1995).

Clearly, the number of crystals that we observe on the oocyte surface is much less than the estimated number of ion channels. This might be explained by a thresholding effect: crystals grow only at the places where channel density is higher, such that the concentration of intracellular Tl^+ exceeds some threshold value. Therefore, the higher the threshold, the fewer crystals would be formed. Our patch-clamp measurements on areas occupied by visible macrocrystals do indeed show that channel density is highest in areas where crystals are formed. Indirect support for the idea that channel organization is indeed clustered is provided by Fig. 7, which shows that the size (area) of TlBr crystals is distributed exponentially, with a very shallow exponential factor. In the absence of more detailed data on crystal shape (which we imagine is a plate beneath the membrane), we can suggest that the top view of the crystal area should be proportional to the number of active channels that contribute to its formation. If we were to assume a random distribution of channels at the membrane, then channel density (and hence crystal size) would be described by the Poisson equation

$$p(n) = \exp(-N_{\mathrm{AVER}})\frac{(N_{\mathrm{AVER}})^n}{n!}$$

where N_{AVER} is the average density of ion channels per unit surface area, and $p(n)$ is the probability of finding n channels within a given unit area. In the current context the most important property of this function is its extremely steep dependence on n. It declines much faster (because of $n!$) than an exponential function when the number of channels in the area exceeds the average. With Kir2.3 channels, the whole-cell current is typically ~10 μA (at −80 mV) with single-channel current amplitude ~1 pA (Makhina et al., 1994), indicating ~10,000,000 channels per cell. If the oocyte surface area is ~10^6 μm^2 (and may be as much as 10-fold more; see, e.g., Zampighi et al., 1995), then the average channel density (ρ) is ~10 channels/μm^2. It follows from experiments that the threshold for crystallization must be higher than ρ, otherwise crystallization would occur over the whole oocyte membrane. Fig. 7 shows that the predicted probability of finding increasingly bigger crystals drops extremely rapidly, even when the threshold for nucleation is about the average channel density (onefold), and declines even faster if the threshold is higher (two- or eightfold). In contrast, the observed distribution of crystal size is very shallow. Thus these experiments indicate that K^+ channels are indeed arranged in clusters on the oocyte membrane.

Polarized distribution of K^+ channels

In contrast to the data on microscopic clustering of K^+ channels, a macroscopic, polarized distribution on the oocyte is quite clear. We have observed two types of polarization in these experiments: a pseudopolarization due to the localization of injected cRNA, and a natural polarization due to some endogenous sorting process in the oocyte. Pseudopolarization was easier to study because it was always present in oocytes injected with cRNA near the membrane surface. Although this phenomenon can be visualized directly with the crystallization method, independent confirmation and quantitative analysis could be made with direct current measurements under voltage clamp, using the agarose-hemiclamp technique developed in this study. Virtually no channels were present on the side opposite that into which the cRNA was injected (Fig. 6). That pseudopolarization is so strong was a surprising finding. A major practical consequence is that directed, not random, cRNA injection may be very useful in controlling the level of channel or other surface protein expression in oocyte studies, for instance, when examining the kinetic response to, say, applied channel agonists and antagonists in whole oocyte voltage-clamp experiments. There is a notoriously slow solution exchange time for such experiments, partly as a result of having portions of the oocyte facing the bottom of the chamber such that solution flow around these regions of the membrane is considerably restricted. Simply injecting cRNA into the one pole and facing this hemisphere up during current measurement may obviate these complications.

We observed an apparently natural polarization in some oocytes, although this phenomenon was less reproducible. As stated above, it was generally observed in most oocytes in a given isolation, or in none. True natural polarization of endogenous calcium-activated chloride channels has been described (Gomez-Hernandez et al., 1997), where current density was ~10 times greater in the animal than in the vegetal pole. This polarization was opposite that which we observed for Kir2.3 currents expressed from RNA injected into the equator. Natural polarization of other structural and membrane proteins has also been demonstrated, e.g., γ-tubulin has been reported to be polarized along the animal-vegetal axis (Gard, 1994). A literature search suggests that although several publications (Lupu-Meiri et al., 1988; Dreyfus et al., 1989; Matus-Leibovitch et al., 1993, 1994; Oron et al., 1993; Yim et al., 1994) have described more or less pronounced hemispheric polarization of proteins or protein functions expressed from injected RNAs, none of these studies explicitly considered the possibility that such polarization might have resulted from polarized injection. In contrast to the natural polarization that we observe, pseudo polarization is a very reproducible phenomenon, and this polarization does not dissipate with time after cRNA injection. Preliminarily, we also find that it is resistant to dissipation by cytoskeletal disrupters like cytochalasin B and colchicine, at concentrations that can be high enough to destroy the hemispheric color pattern of the oocytes.

APPENDIX

The concentration of Tl^+ ions at the exit from a point source can be estimated by assuming steady-state current flow. Integrating the diffusion equation (Eq. 1), where J is ion flux, $S(r)$ is the surface area of a hemisphere, D is the diffusion coefficient, and r is the distance from the point source,

$$J = D \cdot S(r) \frac{dC(r)}{dr} = \text{const.} \quad (1)$$

gives the following estimation of concentration at a distance r_O:

$$C_o = \frac{J}{2\pi D r_o} \quad (2)$$

At a characteristic distance from the center of the pore exit of r_O = 5 Å (i.e., approximately the radius of the real pore), 1 pA current, and ~2×10^{-5} cm^2/s diffusion coefficient for Tl^+ (Hille, 1992, Chapter 10), the estimated concentration of Tl^+ is 1.65 mM. The precipitating concentration of bromide can then be estimated from the solubility product of TlBr salt at room temperature (0.05 g/100 CC ≈ 1.8 mM, from *Handbook of Chemistry and Physics*, 72nd Edition, 1991–1992): $[Br^-] = [1.8\ mM]^2/[Tl] = 1.96$ mM.

This work was supported by grant HL54171 from the National Institutes of Health (CGN), an Established Investigatorship from the American Heart Association (CGN), and a Scientist Development grant from the American Heart Association (ANL).

REFERENCES

Alonso, G., and H. Widmer. 1997. Clustering of Kv4.2 potassium channels in postsynaptic membrane of rat supraoptic neurons: an ultrastructural study. *Neuroscience.* 77:617–621.

Blatz, A. L., and K. L. Magleby. 1984. Ion conductance and selectivity of single calcium-activated potassium channels in cultured rat muscle. *J. Gen. Physiol.* 84:1–23.

Boudier, J. L., T. Le Treut, and E. Jover. 1992. Autoradiographic localization of voltage-dependent sodium channels on the mouse neuromuscular junction using ^{125}I-alpha scorpion toxin. II. Sodium distribution on postsynaptic membranes. *J. Neurosci.* 12:454–466.

Chalfie, M., Y. Tu, G. Euskirchen, W. W. Ward, and D. C. Prasher. 1994. Green fluorescent protein as a marker for gene expression. *Science.* 263:802–805.

Chepilko, S., H. Zhou, H. Sackin, and L. G. Palmer. 1995. Permeation and gating properties of a cloned renal K^+ channel. *Am. J. Physiol.* 268: C389–C401.

Cloues, R., and N. V. Marrion. 1996. Conduction properties of the M-channel in rat sympathetic neurons. *Biophys. J.* 70:806–812.

Deerinck, T. J., S. R. Levinson, G. V. Bennett, and M. H. Ellisman. 1997. Clustering of voltage-sensitive sodium channels on axons is independent of direct Schwann cell contact in the dystrophic mouse. *J. Neurosci.* 17:5080–5088.

Dreyfus, P. A., S. Seidman, M. Pincon-Raymond, M. Murawsky, F. Rieger, E. Schejter, H. Zakut, and H. Soreq. 1989. Tissue-specific processing and polarized compartmentalization of clone-produced cholineserase in microinjected *Xenopus* oocytes. *Cell. Mol. Neurobiol.* 9:323–341.

Eisenman, G., R. Latorre, and C. Miller. 1986. Multi-ion conduction and selectivity in the high-conductance Ca^{++}-activated K^+ channel from skeletal muscle. *Biophys. J.* 50:1025–1034.

Froehner, S. C., C. W. Luetje, P. B. Scotland, and J. Patrick. 1990. The postsynaptic 43K protein clusters muscle nicotinic acetylcholine receptors in *Xenopus* oocytes. *Neuron.* 5:403–410.

Gard, D. L. 1994. Gamma-tubulin is asymmetrically distributed in the cortex of *Xenopus* oocytes. *Dev. Biol.* 161:131–140.

Gomez-Hernandez, J.-M., W. Stuhmer, and A. B. Parekh. 1997. Calcium dependence and distribution of calcium-activated chloride channels in *Xenopus* oocytes. *J. Physiol. (Lond.).* 502:569–574.

Hagiwara, S., S. Miyazaki, S. Krasne, and S. Ciani. 1977. Anomalous permeabilities of the egg cell membrane of a starfish in K^+-Tl^+ mixtures. *J. Gen. Physiol.* 70:269–281.

Hille, B. 1992. Ionic Channels of Excitable Membranes. Sinauer Associates, Sunderland, MA.

John, S. A., J. I. Goldhaber, J. N. Weiss, and B. Ribalet. 1997. Ion channels fused to green fluorescent protein are expressed normally and retain physiological properties. *Biophys. J.* 72:A253.

Kim, E., M. Niethammer, A. Rothschild, Y. N. Jan, and M. Sheng. 1995. Clustering of Shaker-Type K^+ channels by interaction with a family of membrane-associated guanylate kinases. *Nature.* 378:85–88.

Komatsu, H., I. Mori, J. S. Rhee, N. Akaike, and Y. Ohshima. 1996. Mutations in a cyclic nucleotide-gated channel lead to abnormal thermosensation and chemosensation in *C. elegans*. *Neuron.* 17:707–718.

Kume, S., A. Muto, J. Aruga, T. Nakagawa, T. Michikawa, T. Furuichi, S. Nakade, H. Okano, and K. Mikoshiba. 1993. The *Xenopus* IP3 receptor: structure, function, and localization in oocytes and eggs. *Cell.* 73: 555–570.

Lupu-Meiri, M., H. Shapira, and Y. Oron. 1988. Hemispheric asymmetry of rapid chloride responses to inositol trisphosphate and calcium in *Xenopus* oocytes. *FEBS Lett.* 240:83–87.

Makhina, E. N., A. J. Kelly, A. N. Lopatin, R. W. Mercer, and C. G. Nichols. 1994. Cloning and expression of a novel inward rectifier potassium channel from human brain. *J. Biol. Chem.* 269:20468–20474.

Makhina, E. N., and C. G. Nichols. 1998. Independent trafficking of K_{ATP} channel subunits to the plasma membrane. *J. Biol. Chem.* 273: 3369–3374.

Matus-Leibovitch, N., M. C. Gershengorn, and Y. Oron. 1993. Differential effects of cytoskeletal agents on hemispheric functional expression of cell membrane receptors in *Xenopus* oocytes. *Cell. Mol. Neurobiol.* 13:625–637.

Matus-Leibovitch, N., D. R. Nussenzveig, M. C. Gershengorn, and Y. Oron. 1994. The hemispheric functional expression of the thyrotropin-releasing-hormone receptor is not determined by the receptors' physical distribution. *Biochem. J.* 303:129–134.

Oron, Y., R. Vogel, N. Matus-Leibovitch, and M. Aladjem. 1993. The hemispheric distribution of *Torpedo* nicotinic receptors expressed in *Xenopus* oocytes. *J. Basic Clin. Physiol. Pharmacol.* 4:181–197.

Oxford, G. S., and P. K. Wagoner. 1989. The inactivating K^+ current in GH3 pituitary cells and its modification by chemical reagents. *J. Physiol. (Lond.).* 410:587–612.

Palecek, J., V. Habrova, J. Nedvidek, and A. Romanovsky. 1985. Dynamics of tubulin structures in *Xenopus laevis* oogenesis. *J. Embryol. Exp. Morphol.* 87:75–86.

Phillips, W. D., C. Kopta, P. Blount, P. D. Gardner, J. H. Steinbach, and J. P. Merlie. 1991. ACh receptor-rich membrane domains organized in fibroblasts by recombinant 43-kilodalton protein. *Science.* 251:568–570.

Robitaille, R., E. M. Adler, and M. P. Charlton. 1993. Calcium channels and calcium-gated potassium channels at the frog neuromuscular junction. *J. Physiol. (Lond.).* 87:15–24.

Robitaille, R., M. J. Bourque, and S. Vandaele. 1996. Localization of L-type Ca^{2+} channels at perisynaptic glial cells of the frog neuromuscular junction. *J. Neurosci.* 16:148–158.

Scannevin, R. H., H. Murakoshi, K. J. Rhodes, and J. S. Trimmer. 1996. Identification of a cytoplasmic domain important in the polarized expression and clustering of the Kv2.1 K^+ channel. *J. Cell Biol.* 135: 1619–1632.

Shi, G., A. K. Kleinklaus, N. V. Marrion, and J. S. Trimmer. 1994. Properties of Kv2.1 K^+ channels expressed in transfected mammalian cells. *J. Biol. Chem.* 269:23204–23211.

Van Hook, A. 1961. Crystallization. Theory and Practice. Reinhold Publishing, New York.

Veyena-Burke, N., D. Takimoto, K. Li, K. Hoyt, S. Watkins, and E. S. Levitan. 1997. Localization and mobility of GFP-K^+ channel fusion proteins. *Biophys. J.* 72:A351.

Wagoner, P. K., and G. S. Oxford. 1987. Cation permeation through the voltage-dependent potassium channel in the squid axon. Characteristics and mechanisms. *J. Gen. Physiol.* 90:261–290.

Yim, D. L., L. K. Opresko, H. S. Wiley, and R. Nuccitelli. 1994. Highly polarized EGF receptor tyrosine kinase activity initiates egg activation in *Xenopus*. *Dev. Biol.* 162:41–55.

Zampighi, G. A., M. Kreman, K. J. Boorer, D. D. Loo, F. Bezanilla, G. Chandy, J. E. Hall, and E. M. Wright. 1995. A method for determining the unitary functional capacity of cloned channels and transporters expressed in *Xenopus laevis* oocytes. *J. Membr. Biol.* 148:65–78.